STELLAR PHYSICS

Sun-like stars produce superflares roughly once per century

Valeriy Vasilyev[1]*, Timo Reinhold[1], Alexander I. Shapiro[1,2], Ilya Usoskin[3,4], Natalie A. Krivova[1], Hiroyuki Maehara[5], Yuta Notsu[6,7], Allan Sacha Brun[8], Sami K. Solanki[1], Laurent Gizon[1,9]

Stellar superflares are energetic outbursts of electromagnetic radiation that are similar to solar flares but release more energy, up to 10^{36} erg on main-sequence stars. It is unknown whether the Sun can generate superflares and, if so, how often they might occur. We used photometry from the Kepler space observatory to investigate superflares on other stars with Sun-like fundamental parameters. We identified 2889 superflares on 2527 Sun-like stars, out of 56,450 observed. This detection rate indicates that superflares with energies >10^{34} erg occur roughly once per century on stars with Sun-like temperature and variability. The resulting stellar superflare frequency-energy distribution is consistent with an extrapolation of the Sun's flare distribution to higher energies, so we suggest that both are generated by the same physical mechanism.

Solar flares are sudden local bursts of bright electromagnetic emission from the Sun, which release a large amount of energy within a short interval of time (*1*). The increase in short-wavelength solar radiation during flares influences Earth's upper atmosphere and ionosphere, sometimes causing radio blackouts and ionosphere density changes (*2*). Solar flares are frequently accompanied by the expulsion of large volumes of plasma, known as coronal mass ejections (CMEs), which accelerate charged particles to high energies. When these solar energetic particles (SEPs) reach Earth, they cause radiation hazards to spacecraft, aircraft, and humans. Extreme SEP events can produce isotopes, called cosmogenic isotopes, when high-energy particles interact with Earth's atmosphere. These isotopes are then recorded in natural archives, such as tree rings and ice cores (*3*, *4*). The total amount of energy released by each flare varies by many orders of magnitude, as determined by a complex interplay between the physical mechanisms of particle acceleration and plasma heating in the Sun's atmosphere (*5*).

Solar flares have been observed for less than two centuries. Although thousands of them have been detected and measured (*6*–*8*), only about a dozen are known to have exceeded a bolometric (integrated over all wavelengths) energy of 10^{32} erg (*9*, *10*). Among them was the Carrington Event on 1 September 1859 (*11*, *12*), which was accompanied by a CME that had the strongest recorded impact on Earth. Modern estimates of the Carrington Event's total bolometric energy are 4×10^{32} to 6×10^{32} erg (*13*, *14*).

It is unknown whether the Sun can unleash flares with even higher energies, often referred to as superflares, and if so, how frequently that could happen. The period of direct solar observation is too short to reach any firm conclusions. There are two indirect methods to investigate the potential for more intense flares on the Sun. One method uses extreme SEP events recorded in cosmogenic isotope data (*10*, *15*), which have been used to quantify the occurrence rate of strong CMEs reaching Earth over the past few millennia (*4*). There are five confirmed (and three candidate) extreme SEP events that are known to have occurred in the past 10,000 years (*4*), implying a mean occurrence rate of ~10^{-3} year^{-1}. However, the relationship between SEPs and flares is poorly understood, especially for the stronger events (*10*).

A second method is to study superflares on stars similar to the Sun. If the properties of the observed stars sufficiently match the Sun, the superflare occurrence rate on those stars can be used to estimate the rate on the Sun. Studies using this method have indicated that superflares with energies of about 10^{34} erg occur with a frequency of ~$(1.25 \pm 0.87) \times 10^{-3}$ year^{-1} on Sun-like stars (*16*); all uncertainties are 1σ. However, other studies have found substantially lower occurrence rates, probably because of differences in the selection of stars with Sun-like rotation rates (*17*, *18*). For example, one study (*18*) found 26 flares on 15 Sun-like stars (out of 1641 observed), implying an occurrence rate of ~$(3.33 \pm 1.25) \times 10^{-4}$ year^{-1} for a 7×10^{33} erg superflare.

Those previous studies were limited to stars with known rotation periods (*19*). However, the majority of stars with measurable rotation periods are much more variable than the Sun (*20*), potentially biasing the results. Detecting the rotation period of a Sun-like star is challenging using standard methods (*21*, *22*). Therefore, the stars that are most similar to the Sun would have unknown rotation periods and thus were excluded from previous flare studies.

[1]Max-Planck-Institut für Sonnensystemforschung, Göttingen, Germany. [2]Institute of Physics, University of Graz, Graz, Austria. [3]Sodankylä Geophysical Observatory, University of Oulu, Oulu, Finland. [4]Space Physics and Astronomy Research unit, University of Oulu, Oulu, Finland. [5]Subaru Telescope Okayama Branch Office, National Astronomical Observatory of Japan, Okayama, Japan. [6]Laboratory for Atmospheric and Space Physics, University of Colorado Boulder, Boulder, CO, USA. [7]National Solar Observatory, Boulder, CO, USA. [8]Laboratoire Astrophysique Instrumentation and Modélisation, Universities of Paris-Cité and Paris-Saclay, Center for Atomic and Alternative Energies, Center of National Research in Science, Gif-sur-Yvette, France. [9]Institut für Astrophysik, Georg-August-Universität Göttingen, Göttingen, Germany.
*Corresponding author. Email: vasilyev@mps.mpg.de

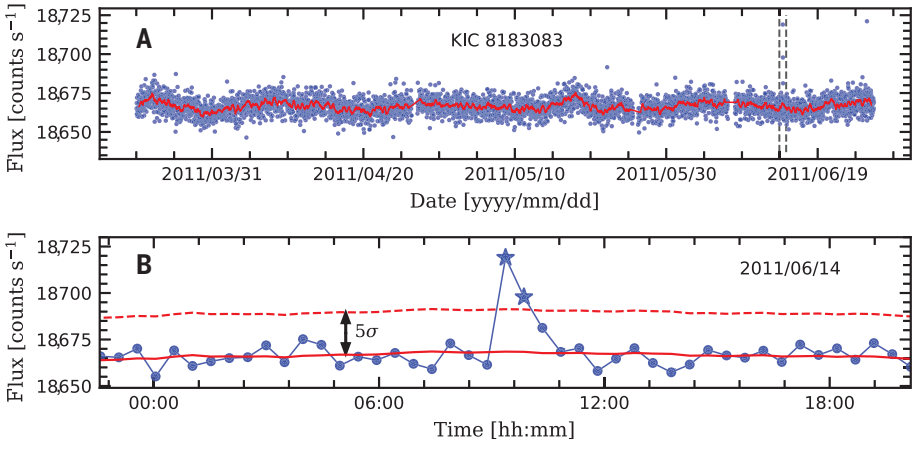

Fig. 1. Example superflare light curve. (**A**) Observed light curve of the Sun-like star KIC 8183083 (blue dots) and the same data smoothed with a 7.5-hour window (red curve). The vertical dashed lines enclose a superflare identified by our automated algorithm. (**B**) Zoom into the region between the dashed lines in (A). Star symbols indicate data points >5σ above (dashed red line) the smoothed light curve. The uncertainties in the flux values are smaller than the size of the data points.

Downloaded from https://www.science.org at Oulu University on December 12, 2024

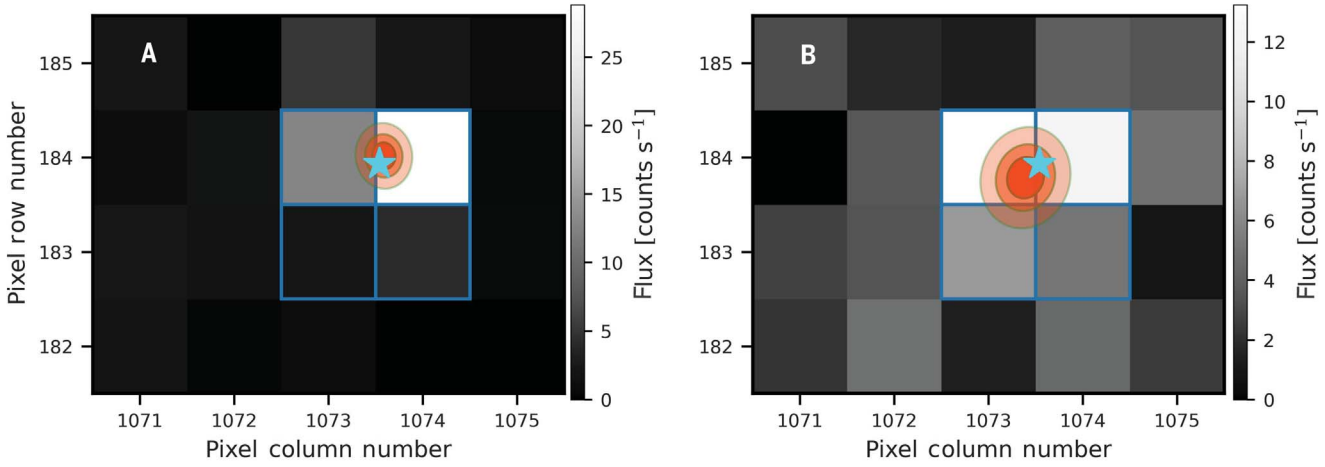

Fig. 2. Spatial localization of the example superflare. (**A**) Kepler image of the same flare on KIC 8183083 as in Fig. 1 during the maximum flare light. (**B**) The same flare 30 min later. Grayscale (see color bar) indicates the flux in each pixel during the flare. The blue outlines indicate the four pixels used to extract the light curve (shown in Fig. 1), and the cyan star is the catalog position of the star (*25*). The orange ellipses indicate the 68, 95, and 99.9% confidence levels obtained by fitting a model of a point source to those images. The star is located within the 99.9% confidence contour in both images, so we attribute the flare in the light curve to this target.

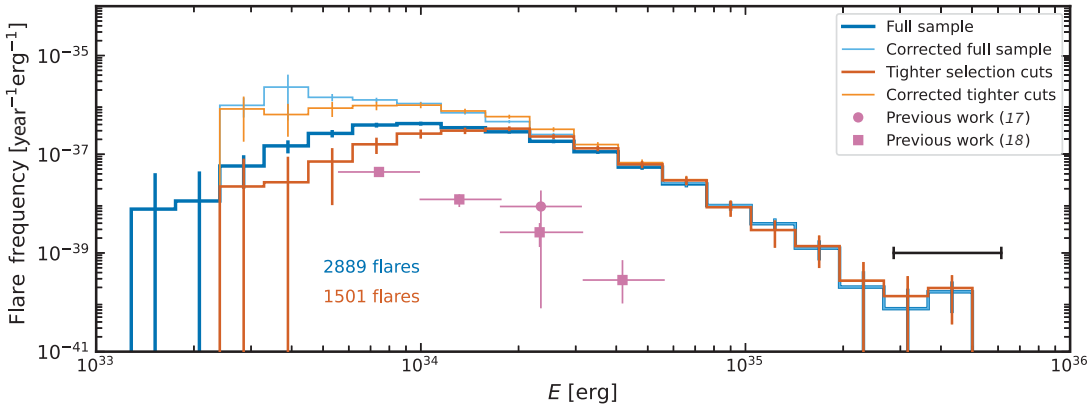

Fig. 3. Frequency-energy distribution of stellar flares. The thick blue histogram shows the flare frequency—the number of flares per star per year per unit energy—of all stars in our full sample as a function of the flare energy. The thick orange histogram shows the results for our sample with tighter selection cuts (effective temperatures 5500 to 6000 K and variabilities R_{var} < 0.3%). The thin blue and thin orange curves show the same distributions after correction for the missing low-energy flares caused by the detection threshold (*23*). The error bars on each histogram bin show 1σ uncertainties (*23*). Results from previous studies are shown as pink circles (*17*) and squares (*18*). The black horizontal error bar indicates the typical 1σ uncertainty in stellar flare energy.

Downloaded from https://www.science.org at Oulu University on December 12, 2024

Kepler observations of superflares

We searched for superflares on Sun-like stars observed by the Kepler space telescope. We chose to include stars with unknown rotation periods in the analysis (*23*). Our sample consists of main-sequence stars with near-solar fundamental parameters, selected on the basis of effective temperatures 5000 K < T_{eff} < 6500 K and G-band absolute magnitudes 4 mag < M_G < 6 mag taken from the Kepler archive (*24*), supplemented with data from Gaia Data Release 3 (DR3) (*25*). For context, the Sun has an effective temperature $T_{eff}^{\odot} = 5780$ K and an absolute magnitude $M_G^{\odot} = 4.66$ mag. We used Gaia astrometry to exclude unresolved binary systems with semimajor axes greater than 0.1 astronomical units (*23*, *26*). We excluded stars with known rotation periods shorter than 20 days (*23*) using a rotation period catalog (*27*). These stars are probably younger than the Sun (which has a rotation period of 25 days) and therefore more active, resulting in a higher flare frequency, which could bias the measured superflare frequency.

We applied an automated flare detection algorithm (*28*) to these stars. The method uses a combined analysis of the light curve (observed stellar brightness as a function of time) and images to identify flare locations on the detector with subpixel precision. All stars in our sample were observed by the Kepler mission with a 30-min exposure time, so a typical superflare profile consisted of only a few data points (Fig. 1). To detect superflares with high statistical confidence, we searched for events with at least two consecutive data points that exceed the background by at least a 5σ threshold. Each data point in the stellar light curve corresponds to the photon flux integrated over a particular pixel mask around the target star. In some cases, the light curve is affected by events not related to the target star, such as cosmic rays, flares on (un)resolved background stars, and minor Solar System bodies passing through the field of view. Although we expect such contamination to be rare, it might strongly affect the flare statistics of stars with low flare occurrence rates. Therefore, we additionally analyzed the images (*23*) corresponding to the first two data points exceeding the 5σ threshold in each light curve to spatially localize the flare source (Fig. 2). Our algorithm fits a model of a point source to those images and localizes the flare on a subpixel level. If the target Sun-like star resides within the 99.9% confidence ellipse of the probable flare location, we attribute the flare to that star.

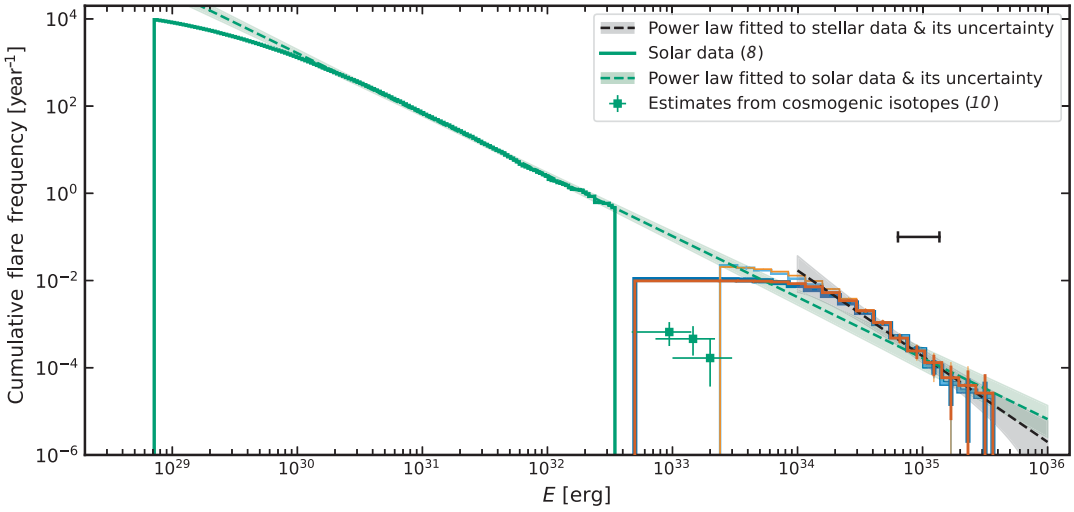

Fig. 4. Cumulative frequency-energy distributions of solar and stellar flares. The orange and blue histograms show cumulative data for the same samples as in Fig. 3. The black dashed line is a power law function fitted to the distribution of stellar flares with energies >10^{34} erg. The green histogram shows the cumulative distribution of flares on the Sun between 1986 and 2020 (*8*, *23*). The green dashed line is an extrapolation from the distribution of solar flares with energies 10^{30} to 10^{32} erg. The green squares indicate the cumulative distribution of extreme SEP events on the Sun inferred from cosmogenic isotopes (*10*). The black horizontal error bar indicates the typical 1σ uncertainty in stellar flare energy.

We examined the light curves of stars with multiple flares to exclude potential contamination of our sample by fast rotators (*23*) that were not reported in the catalog (*27*). In total, we analyzed 56,450 stars, of which 39,347 stars had unknown rotation periods and 17,103 had measured rotation periods (*27*); from that sample, we identified 2889 flares on 2527 stars. The bolometric flare energies range from ~10^{33} to ~10^{36} erg (*23*). With 4 years of observations for each star, our full sample corresponds to ≈220,000 years of stellar activity—roughly 18 times longer than the cosmogenic isotope record of the Sun [which covers ≈12,000 years (*4*)].

Flare frequency distribution

We determined (*23*) the flare frequency as a function of the flare energy, E, to quantify the number of flares per star per year per unit of energy. Figure 3 shows our calculated stellar flare frequency, and Fig. 4 shows its associated cumulative distribution. Above 10^{34} erg, the stellar superflare frequency decreases with energy, roughly following a power law, $\sim E^{-\alpha}$, where α is the power-law exponent. Fitting a power law model to the cumulative distribution gives $\alpha = 1.97 \pm 0.30$ (Fig. 4).

Our measured frequency of stellar superflares with energies <10^{34} erg is incomplete, because their signal-to-noise ratios could fall below our detection threshold (*23*, *28*). For the Sun, the cumulative distribution of flares also follows a power law (*8*, *29*), with $\alpha = 1.399 \pm 0.056$ (*23*) over a lower energy range (10^{29} to 10^{33} erg). Although the solar and stellar measurements do not overlap in energy, an extrapolation of the solar flare frequency distribution to higher energies is consistent with the stellar superflare frequency distribution (Fig. 4).

The cumulative distribution of stellar superflares indicates that Sun-like stars with effective temperatures between 5000 and 6500 K generate superflares with energies greater than 10^{34} erg with a frequency of $(8.63 \pm 0.20) \times 10^{-3}$ year^{-1}. This stellar sample includes stars both slightly cooler and warmer than the Sun as well as stars that are currently more variable than the Sun has been at any point in the past 140 years (*20*). We quantified the stellar variability using the variability range R_{var}, computed as the difference between the 95th and 5th percentiles of the fluxes in a light curve, which are sorted in increasing order and normalized by their median (*20*, *30*, *31*). We found that narrowing the stellar sample to stars more similar to the Sun—temperatures 5500 to 6000 K and variabilities within the solar range, $R_{var} < 0.3\%$ (*20*)—had very little effect on the superflare frequency (Fig. 4). Further narrowing this sample to stars with known rotation periods reduced the number of stars by almost a factor of six but had minimal impact on measured flare frequency. Table 1 lists our measured flare frequencies for three different sample selection cuts, along with the Sun for comparison.

Comparison to previous results

Previous studies of stellar superflares (*17*, *18*, *32*) also found that the flare frequency follows a power law as a function of energy. However, those studies found frequencies approximately two orders of magnitude lower than our measurements (Fig. 3), inconsistent with an extrapolation of the solar flare distribution to higher energies. We attribute this difference to three main factors:

1) Our method accounts for possible contamination by flares on background stars, cosmic rays, and minor Solar System bodies. We therefore did not need to restrict our stellar sample to isolated stars (those without nearby background sources). Previous studies (*18*, *32*) excluded ~70% of Sun-like stars from their analysis for this reason. Removing this requirement allowed us to use a larger sample size.

2) Previous studies used a higher flare detection threshold in their light curve analysis to exclude background events (*32*). We expected our algorithm for subpixel localization of flares in the Kepler images to filter out those background events, so we set a lower flare detection threshold of a 5σ peak in the light curve.

3) Previous studies (*33*) argued that very large star spots, with an area of >10^{-2} of the stellar hemisphere, are required to generate superflares. They expected such large star spots to produce large photometric variability, sufficient to determine the rotation period. Previous studies therefore assumed that stars with unknown rotation periods (~84% of those with Sun-like effective temperatures) are inactive and excluded them from their samples. Our analysis identified 1941 superflares that occurred on stars with unknown rotation periods and low variability ($R_{var} < 0.3\%$) (*23*), which would have been excluded from previous studies. The low photometric variability of those stars does not imply the absence of large star spots. Photometric variability is strongly affected by the nonaxisymmetry of the surface spot distribution (*34*, *35*), stellar inclination angles (*36*), and bright facular features that can reduce photometric variability by compensating for spot contribution (*37*, *38*). We discuss these differences in more detail in the supplementary text in the supplementary materials. This combination of factors means that we measured a higher stellar superflare frequency than previous studies (Fig. 3).

Downloaded from https://www.science.org at Oulu University on December 12, 2024

Table 1. Measured superflare frequencies. The flare frequencies derived from our measurements are listed for two energy ranges and three stellar sample selection cuts. Uncertainties are 1σ. N_{flares} is the number of detected flares, N_{stars} is the number of stars they occurred on, and P_{rot} is the rotation period. For comparison, we also list values for the Sun extrapolated from solar flares at lower energies.

Sample selection	Number of stars in sample	Frequency (year^{-1}) 10^{34} to 10^{35} erg	Frequency (year^{-1}) $E > 10^{35}$ erg	N_{flares}	N_{stars}
G-type main-sequence stars 5000 K < T_{eff} < 6500 K P_{rot} > 20 days or unknown	56,450	$(8.63 \pm 0.20) \times 10^{-3}$	$(3.90 \pm 0.60) \times 10^{-4}$	2889	2527
G-type main-sequence stars 5500 K < T_{eff} < 6000 K R_{var} < 0.3% P_{rot} > 20 days or unknown	32,450	$(9.31 \pm 0.30) \times 10^{-3}$	$(3.59 \pm 1.06) \times 10^{-4}$	1501	1383
G-type main-sequence stars 5500 K < T_{eff} < 6000 K R_{var} < 0.3% 20 days < P_{rot} < 30 days	5,959	$(7.70 \pm 0.95) \times 10^{-3}$	–	238	208
The Sun	–	$\left(4.13^{+1.95}_{-1.38}\right) \times 10^{-3}$	$\left(1.63^{+1.18}_{-0.76}\right) \times 10^{-4}$	–	–

Implications for the Sun

We found that Sun-like stars produce superflares with bolometric energies of $>10^{34}$ erg roughly once per century. That is more than an order of magnitude more energetic than any solar flare recorded during the space age, which spans about 60 years. Between 1996 and 2012, 12 solar flares had bolometric energies of $>10^{32}$ erg, but none were $>10^{33}$ erg (*9*). The most powerful solar flare recorded occurred on 28 October 2003, with an estimated bolometric energy of 7×10^{32} erg (*9*, *39*), which exceeds estimates for the Carrington Event (4×10^{32} to 6×10^{32} erg) (*13*, *14*). We also found that our measured stellar superflare frequency and the solar flare distribution extrapolated to higher energies are consistent with each other, having similar power law distributions and indices α, which might indicate a shared (super)flare generation mechanism.

The number of extreme SEP events identified in the cosmogenic isotopes record of the past 12 millennia (*40*) is substantially lower than that implied by the superflare frequency of the Sun from either the extrapolation of solar flare data or our stellar superflare measurements (Fig. 4). It is unlikely that extreme SEP events have been overlooked in cosmogenic isotope data (*41*), so this inconsistency could be due to the indirect connection between SEP events and superflares. The relationship between the energies of SEP events and superflares is highly uncertain (*10*) (see supplementary text). It is possible that superflares are rarely accompanied by extreme SEP events, as has been found for lower-energy solar flares (*42*).

We cannot exclude the possibility that there is an inherent difference between flaring and nonflaring stars that was not accounted for by our selection criteria. If so, the flaring stars in the Kepler observations would not be representative of the Sun. Approximately 30% of flaring stars are known to have a binary companion (*17*, *23*). Flares in those systems might originate on the companion star or be triggered by tidal interactions. If, instead, our sample of Sun-like stars is representative of the Sun's future behavior, it is substantially more likely to produce a superflare than was previously thought.

REFERENCES AND NOTES

1. A. O. Benz, *Living Rev. Sol. Phys.* **14**, 2 (2017).
2. A. P. Mitra, in *Ionospheric Effects of Solar Flares*, vol. 46 of *Astrophysics and Space Science Library* (D. Reidel Publishing Company, 1974), pp. 126–146.
3. F. Miyake, I. Usoskin, S. Poluianov, Eds., *Extreme Solar Particle Storms: The Hostile Sun* (IOP Publishing, 2019).
4. I. G. Usoskin, *Living Rev. Sol. Phys.* **20**, 2 (2023).
5. N. Gopalswamy, in *Extreme Events in Geospace: Origins, Predictability, and Consequences*, N. Buzulukova, Ed. (Elsevier, 2018), pp. 37–63.
6. A. Veronig, M. Temmer, A. Hanslmeier, W. Otruba, M. Messerotti, *Astron. Astrophys.* **382**, 1070–1080 (2002).
7. M. J. Aschwanden, S. L. Freeland, *Astrophys. J.* **754**, 112 (2012).
8. N. Plutino, F. Berrilli, D. Del Moro, L. Giovannelli, *Adv. Space Res.* **71**, 2048–2058 (2023).
9. A. G. Emslie *et al.*, *Astrophys. J.* **759**, 71 (2012).
10. E. W. Cliver, C. J. Schrijver, K. Shibata, I. G. Usoskin, *Living Rev. Sol. Phys.* **19**, 2 (2022).
11. R. C. Carrington, *Mon. Not. R. Astron. Soc.* **20**, 13–15 (1859).
12. R. Hodgson, *Mon. Not. R. Astron. Soc.* **20**, 15–16 (1859).
13. E. W. Cliver, W. F. Dietrich, *J. Space Weather Space Clim.* **3**, A31 (2013).
14. H. Hayakawa *et al.*, *Astrophys. J. Lett.* **954**, L3 (2023).
15. F. Miyake, K. Nagaya, K. Masuda, T. Nakamura, *Nature* **486**, 240–242 (2012).
16. H. Maehara *et al.*, *Nature* **485**, 478–481 (2012).
17. Y. Notsu *et al.*, *Astrophys. J.* **876**, 58 (2019).
18. S. Okamoto *et al.*, *Astrophys. J.* **906**, 72 (2021).
19. A. McQuillan, T. Mazeh, S. Aigrain, *Astrophys. J. Suppl. Ser.* **211**, 24 (2014).
20. T. Reinhold *et al.*, *Science* **368**, 518–521 (2020).
21. E. M. Amazo-Gómez *et al.*, *Astron. Astrophys.* **636**, A69 (2020).
22. T. Reinhold *et al.*, *Astrophys. J. Lett.* **908**, L21 (2021).
23. Materials and methods are available as supplementary materials.
24. S. E. Thompson *et al.*, "Kepler Data Release 25 Notes," Tech. Rep. KSCI-19065-002 (NASA Ames Research Center, 2016).
25. Gaia Collaboration, *Astron. Astrophys.* **674**, A1 (2023).
26. V. Belokurov *et al.*, *Mon. Not. R. Astron. Soc.* **496**, 1922–1940 (2020).
27. T. Reinhold, A. I. Shapiro, S. K. Solanki, G. Basri, *Astron. Astrophys.* **678**, A24 (2023).
28. V. Vasilyev *et al.*, *Astron. Astrophys.* **668**, A167 (2022).
29. C. J. Schrijver *et al.*, *J. Geophys. Res. Space Phys.* **117**, A08103 (2012).
30. G. Basri *et al.*, *Astrophys. J. Lett.* **713**, L155–L159 (2010).
31. G. Basri *et al.*, *Astron. J.* **141**, 20 (2011).
32. T. Shibayama *et al.*, *Astrophys. J. Suppl. Ser.* **209**, 5 (2013).
33. K. Shibata *et al.*, *Publ. Astron. Soc. Jpn.* **65**, 49 (2013).
34. E. Işık, A. I. Shapiro, S. K. Solanki, N. A. Krivova, *Astrophys. J. Lett.* **901**, L12 (2020).
35. I. S. Narrett, B. V. Rackham, J. de Wit, *Astron. J.* **167**, 107 (2024).
36. N. E. Nèmec, A. I. Shapiro, E. Işık, S. K. Solanki, T. Reinhold, *Astron. Astrophys.* **672**, A138 (2023).
37. A. I. Shapiro *et al.*, *Nat. Astron.* **1**, 612–616 (2017).
38. T. Reinhold, K. J. Bell, J. Kuszlewicz, S. Hekker, A. I. Shapiro, *Astron. Astrophys.* **621**, A21 (2019).
39. C. S. Moore, P. C. Chamberlin, R. Hock, *Astrophys. J.* **787**, 32 (2014).
40. I. Usoskin *et al.*, *Space Sci. Rev.* **219**, 73 (2023).
41. I. G. Usoskin *et al.*, *Astron. Astrophys.* **670**, L22 (2023).
42. T. Li *et al.*, *Astrophys. J.* **900**, 128 (2020).
43. J. V. d. M. Cardoso *et al.*, Lightkurve: Kepler and TESS time series analysis in Python (Astrophysics Source Code Library, 2018).
44. V. Vasilyev, Flare detection algorithm, version 1.0.2, Zenodo (2024); https://doi.org/10.5281/zenodo.13951243.

ACKNOWLEDGMENTS

We thank the three anonymous referees for constructive criticism and useful advice, which greatly improved the paper. Data collected by the Kepler mission were obtained from the Mikulski Archive for Space Telescopes (MAST) operated by the Space Telescope Science Institute (STScI). Funding for the Kepler mission is provided by the NASA Science Mission Directorate. STScI is operated by the Association of Universities for Research in Astronomy, Inc., under NASA contract NAS 5–26555. Data from the European Space Agency (ESA) mission Gaia (https://www.cosmos.esa.int/gaia) were processed by the Gaia Data Processing and Analysis Consortium (DPAC; https://www.cosmos.esa.int/web/gaia/dpac/consortium). Funding for the DPAC has been provided by national institutions, in particular the institutions participating in the Gaia Multilateral Agreement. This research

Downloaded from https://www.science.org at Oulu University on December 12, 2024

made use of Lightkurve, a Python package for Kepler and TESS data analysis (*43*). **Funding:** V.V. and L.G. acknowledge support from the Max Planck Society under grant "Preparations for PLATO Science" and from the German Aerospace Center (DLR) under grant "PLATO Data Center" 50OP1902. A.I.S. acknowledges funding from European Research Council Synergy Grant REVEAL 101118581. A.S.B. and L.G. acknowledge funding from European Research Council Synergy Grant WHOLE SUN 810218. A.S.B. acknowledges financial support by grants from CNES Solar Orbiter and Space Weather and CNRS-INSU/PNST. T.R. acknowledges support from German Aerospace Center (DLR) grant 50OU2101. I.U. acknowledges support from the Research Council of Finland (projects 321882 and 354280). Y.N. acknowledges support from NASA ADAP award program 80NSSC21K0632, Japan Society for the Promotion of Science (JSPS) KAKENHI grant 21J00106, and the International Space Science Institute, which supports International Team 510, "Solar Extreme Events: Setting Up a Paradigm." H.M. was supported by JSPS KAKENHI grants JP20H05643, JP21H01131, JP24K00685, JP24H00248, and 24K00680. **Author contributions:** V.V., A.I.S., S.K.S., and I.U. conceived of the study. A.I.S., S.K.S., and N.A.K. supervised the project. V.V. and T.R. analyzed the Kepler and Gaia data and obtained the final results. V.V. wrote the software. All authors contributed to the methodology, interpretation, and manuscript preparation. **Competing interests:** There are no competing interests to declare. **Data and materials availability:** The stars we selected for our sample are listed in data S1, and the flares we identified are listed in data S2. The Kepler light curves and images (target pixel files) are available from MAST at https://archive.stsci.edu/kepler/data_search/search.php or using the Lightkurve package (*43*), in either case using the Kepler IDs listed in data S1. The Gaia data are available through the ESA Gaia Archive at https://gea.esac.esa.int/archive/ by selecting "single object" then using the Gaia DR3 IDs in data S1. The flare detection code (*28*) is available at https://github.com/ValeriyVasilyevAstro/LOSE and archived in Zenodo (*44*). **License information:** Copyright © 2024 the authors, some rights reserved; exclusive licensee American Association for the Advancement of Science. No claim to original US government works. https://www.science.org/about/science-licenses-journal-article-reuse. This research was funded in whole or in part by the Research Council of Finland (321882 and 354280), a cOAlition S organization. The author will make the Author Accepted Manuscript (AAM) version available under a CC BY public copyright license.

SUPPLEMENTARY MATERIALS

science.org/doi/10.1126/science.adl5441
Materials and Methods
Supplementary Text
Figs. S1 to S7
Table S1
References (*45*–*67*)
Data S1 and S2

Submitted 27 January 2024; accepted 31 October 2024
10.1126/science.adl5441

Downloaded from https://www.science.org at Oulu University on December 12, 2024